JOURNAL OF GEOPHYSICAL RESEARCH, VOL. 115, D13105, doi:10.1029/2009JD013353, 2010

Horizontal cascade structure of atmospheric fields determined from aircraft data

S. Lovejoy,[1] A. F. Tuck,[2] and D. Schertzer[3,4]

Received 7 October 2009; revised 15 October 2009; accepted 2 February 2010; published 10 July 2010.

[1] Aircraft measurements of the power spectra of the horizontal wind field typically find a transition from $\approx k^{-5/3}$ to $\approx k^{-2.4}$ at scales somewhere around 40 km (k is a wave number). In the usual interpretation this represents a transition between an isotropic three-dimensional (3-D) ($k^{-5/3}$) and an isotropic 2-D (k^{-3}) turbulence; we have recently argued that the turbulence is so highly anisotropic that it has different exponents in the horizontal and vertical. When coupled with gently sloping isobaric aircraft trajectories this predicts the break as a transition from a roughly horizontal spectrum at small scales to the spurious appearance of the vertical spectrum at large scales. If the atmosphere indeed has wide-range horizontal scaling, then it is important to test out the multiplicative cascade models that predict its statistical behavior. In this paper, we do this by analyzing wind, temperature, pressure, and humidity data from the Winter Storm 2004 experiment using 24 aircraft legs, each 1120 km long and at 280 m resolution. We analyze both the turbulent fluxes and the fluctuations showing that in spite of the nonflat trajectories, there is good evidence of roughly planetary-scale multiplicative cascades. By carefully determining the scale-by-scale effects of intermittency on the aircraft altitude and measurements, we estimate the corresponding scaling exponents. We argue that our results should finally permit the emergence of a long-needed consensus about the basic scale-by-scale statistical properties of the atmosphere. They also point to the urgent need to develop anisotropic scaling models of turbulence.

Citation: Lovejoy, S., A. F. Tuck, and D. Schertzer (2010), Horizontal cascade structure of atmospheric fields determined from aircraft data, *J. Geophys. Res.*, *115*, D13105, doi:10.1029/2009JD013353.

1. Introduction

1.1. Reinterpreting the Statistics of the Horizontal Wind

[2] Data analysis requires a theoretical framework in which the physical quantities can be defined and understood. In the case of aircraft measurements of atmospheric turbulence, it is usual to interpret the measurements in an isotropic or quasi-isotropic framework in which the basic exponents are the same in the horizontal and vertical directions. However, starting in the 1980s, studies of the vertical structure of the atmosphere have almost invariably concluded that the horizontal wind is scaling in the vertical, but with a different exponent than in the horizontal. This empirically observed scaling stratification has thus been interpreted either with quasi-linear gravity wave models [*VanZandt*, 1982; *Gardner*, 1994; *Gardner et al.*, 1993; *Dewan*, 1997; *Koch et al.*, 2005] or the 23/9D strongly turbulent model [*Schertzer and Lovejoy*, 1985; *Lovejoy et al.*, 2008b].

[3] In the last few years, these results have prompted the examination of the consequences of such anisotropic but scaling turbulence for the interpretation of aircraft data; both for stratospheric aircraft following isomachs [*Lovejoy et al.*, 2004] and for tropospheric aircraft following isobars (or other gradually sloping trajectories) [*Lovejoy et al.*, 2009c]. The perhaps surprising conclusions were that they are best explained by a single wide-range anisotropic scaling regime. A corollary is that the usual interpretation, that the atmosphere has two (or more) isotropic scaling regimes (e.g., small-scale, three-dimensional (3-D) isotropic and large-scale, 2-D isotropic), is untenable. The key finding was that when measuring the wind field, rather than detecting successively two different isotropic turbulence exponents, the aircraft first detects at small scales the correct horizontal exponent, and then, at larger scales where the departure of the aircraft from a roughly flat to a sloping trajectory becomes important, it spuriously measures the different vertical exponent. In terms of traditional spectral exponents β, (i.e., the spectra are of the form $E(k) \approx k^{-\beta}$ where k is a wave number), the horizontal has $\beta \approx 5/3$ (near the Kolmogorov value) while the vertical has $\beta \approx 2.4$. More precisely, as accurately estimated by drop sondes [*Lovejoy et al.*, 2007], β increases roughly monotonically from about 2.15 ± 0.04 near the surface to 2.51 ± 0.04 at 10 km altitude; see Figure 1c. The near surface value is, to within intermittency corrections, that predicted for buoyancy driven turbulence by *Bolgiano* [1959]

[1]Department of Physics, McGill University, Montreal, Quebec, Canada.
[2]Visiting professor at Department of Physics, Imperial College London, London, UK.
[3]CEREVE, Université Paris Est, Marne-la-Vallee, France.
[4]Météo France, Paris, France.

0148-0227/10/2009JD013353

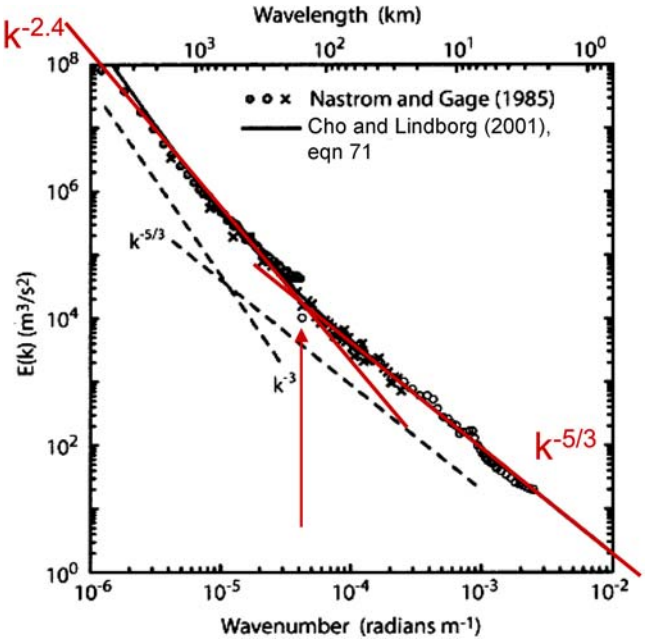

Figure 1a. An intercomparison of the GASP and MOZAIC spectra from commercial aircraft flying on isobars, adapted from *Skamarock* [2004]. The red lines show the behavior predicted if the atmosphere has a perfect $k^{-5/3}$ horizontal spectrum but estimated from an aircraft following roughly horizontal trajectories until about 100 km and then following gradually sloping trajectories (either on isobars or gradual changes in altitude due to fuel consumption).

and *Obukhov* [1959] and the error bars indicate the spread between the mean sonde to sonde exponent and the overall regression exponent using 235 sondes.

[4] As pointed out by *Lilley et al.* [2008] and especially *Lovejoy et al.* [2009c], the slightly larger upper troposphere values 2.4–2.5 are almost exactly the same as the values of the large-scale exponents found in all the major aircraft campaigns including GASP [*Nastrom and Gage*, 1985], MOZAIC [*Cho and Lindborg*, 2001] and others [*Gao and Meriwether*, 1998; *Bacmeister et al.*, 1996]. Figure 1a adapted from *Skamarock* [2004] neatly compares on a single graph, the two largest aircraft campaigns to date: GASP and MOZAIC. It can be seen that, as predicted, at scales of about ≈ 100 km the exponents shift from the small-scale Kolmogorov value $\beta \approx 5/3$ to the vertical value $\beta \approx 2.4$. The spectra in Figure 1a are extremely close to those given by *Lovejoy et al.* [2009c] using the same data as below (see Figure 4c in section 4.1.1), except that the transition scale (which varies greatly from trajectory to trajectory) is on average ≈ 40 km rather than ≈ 100–200 km. We should note that the persistence of a $k^{-5/3}$ regime to such large scales is a fundamental problem for the standard 2-D/3-D model since at those scales the turbulence cannot be isotropic. Various speculative mechanisms to explain it include the description "escaped" 3-D energy transformed to quasi-2-D stratified turbulence [*Lilly*, 1989], "squeezed 3D isotropic turbulence" [*Högström et al.*, 1999] and "upscale quasi-2D nonlinear KE cascades from smaller scales where the KE is stirred by moist convection" [*Takahashi et al.*, 2006]. Other unsatisfactory features are the unknown flux sinks in the 2-D/3-D transition region, an unknown large-scale energy flux dissipation mechanism (surface drag?), and speculative energy and enstrophy flux sources at ≈ 2000 km.

[5] These empirical results can be explained if atmospheric dynamics are scaling but strongly anisotropic, i.e., with different exponents in the horizontal and vertical directions. To put this anisotropic model in perspective, recall that the classical model of atmospheric motions first postulates isotropy (in either two or three dimensions) and only then scaling. Since the troposphere is only ≈ 10 km thick large structures must be "flattened"; that such isotropic models therefore require at least two scaling regimes, the usual ones being dominated by energy flux (leading to a small-scale Kolmogorov, $\beta = 5/3$ regime) and a large-scale ($\beta = 3$) enstrophy flux dominated regime (actually such models require a third even larger-scale $\beta = 5/3$ inverse energy flux cascade regime, but this is rarely discussed). This classical model has been dominant ever since *Charney* [1971] extended *Kraichnan*'s [1967] pure hydrodynamic two dimensional turbulence model to quasi-geostrophic turbulence. In comparison, the anisotropic scaling model implies that the stratification increases in a power law manner so that structures 20,000 km long in the horizontal may only be 10 km thick in the vertical. It turns out that all that is required to obtain a spurious $k^{-2.4}$ regime is a small mean aircraft slope with respect to the horizontal, for example, due to a slow rise due to fuel consumption, or along an isobaric surface. If the isobars were sufficiently rough, then following an isobar might lead to yet another behavior. However, isobars and geopotentials are very smooth. More precisely, if their spectral slopes β are greater than 3 (as in, e.g., work by *Trenberth and Solomon* [1993]), then their RMS variability is due to low not high wave numbers, so $\beta > 3$ is at least a rough criterion for "smooth enough" suggesting that sloping isobars and straight sloping trajectories will yield the same behavior.

[6] As model resolutions increased, the predictions of this standard 2-D/3-D model could be directly tested numerically, at least at the large scales. The first tests [*Chen and Wiin-Nielsen*, 1978; *Boer and Shepherd*, 1983] had very small ranges of scales and are widely cited as giving support to 2-D turbulence, especially its prediction of a k^{-3} regime. However, given the long history of "shoe-horning" atmospheric spectra into a k^{-3} mold, reexamination of their original results is salutary; see the *Boer and Shepherd* [1983] key result in Figure 1b which shows the enstrophy spectrum ($= k^2E(k) = k^{2-\beta}$). We see that although for $k > 5$ the vertically integrated and transient spectra are very close to $\beta = 2.4$, the stationary spectrum is close to $\beta \approx 4$, with no indication of a $\beta \approx 3$ regime. This prompted the following prescient comment: "For the purposes of comparison with theory, the spectral slopes obtained from the data are somewhat shallower than the values of −3 suggested by simple theory. It must be emphasized however, the enstrophy containing inertial subrange is not really a prediction for the atmosphere but is a possible solution to the spectral equation in an unforced subrange which may or may not have some correspondence to the situation in the real atmosphere" [*Boer and Shepherd*, 1983]. They continue: "Consequently, the fact that the spectra obey power laws at all may be considered to be a striking, although by now well known feature of the atmosphere." This primacy of the scale invariance symmetry, albeit a strongly anisotropic one, is the basis of the alternative discussed here.

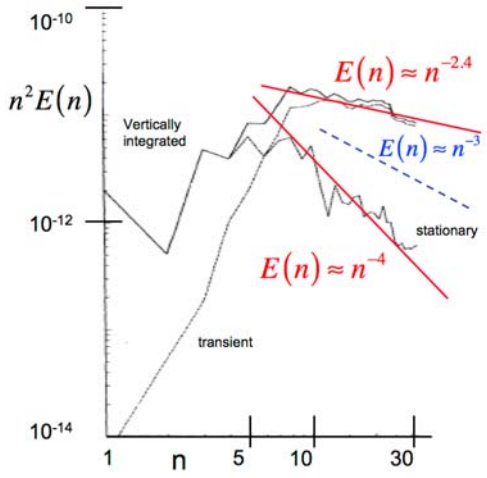

Figure 1b. The enstrophy spectrum ($= n^2E(n)$ where $E(n)$ is the wind spectrum and n is the principal spherical harmonic wave number), adapted from *Boer and Shepherd* [1983]. The three curves are from January data; the top solid line is for the vertically integrated atmosphere, the dashed line indicates "stationary" (the spatial spectrum of the monthly average), and the dotted transient line is the deviation from the monthly average. We have added reference lines with slopes −2.4, −3, and −4. Over the range $n \approx 5$ to 30 (700–4000 km) the exponents of the spectra of the transient and vertically averaged atmosphere are extremely close to the vertical value $\beta \approx 2.4$, but the stationary spectrum exponent is $\beta \approx 4$. No $\beta \approx 3$ regime is observed.

Later, *Strauss and Ditlevsen* [1999] applied the same *Boer and Shepherd* [1983] 2-D analysis framework to much higher resolution ERA 40 reanalyses also finding "roughly $\beta \approx 2.5$–2.7… this slope is significantly different than the classical turbulence theory prediction of 3" a fact which they partially attribute to a "lack of an enstrophy cascade."

[7] Today, we can revisit wind spectra using the state-of-the-art successor to the *Strauss and Ditlevsen* [1999] data, the ECMWF interim reanalysis, and calculate the spectrum directly without Strauss and Ditlevsen's, complex 2-D preprocessing. Figure 1c shows the isotropic spectrum of the zonal wind at each tropospheric 100 mbar level, compensated by the average $k^{-2.4}$ behavior so as to accentuate the small deviations. Also shown in Figure 1c are straight reference lines. These are not regressions but rather the predictions of the model presented here: the slopes are those empirically estimated in the vertical direction from drop sondes [*Lovejoy et al.*, 2007]. Regressions on the reanalysis spectra from $k = 2$ to $k = 30$ give β differing by less than 0.05 throughout the data rich lower 4 km, rising to only 0.2 at 10 km ($\approx$ 200 mbar). These small differences could easily be the consequence of either intermittent aircraft and/or sonde motion; see below. For reference, the exact values at 100 mbar levels are: (1000, 2.15, 2.16), (900, 2.29, 2.26), (800, 2.36, 2.32), (700, 2.38, 2.40), (600, 2.40, 2.48), (500, 2.43, 2.53), (400, 2.47, 2.62), (300, 2.52, 2.68), (200, 2.45, 2.82) for (pressure in mbars, drop sonde β, horizontal reanalysis β).

[8] A possible explanation for the difficulties with the standard 2-D/3-D picture comes from work by *Bartello*, 1995] and *Ngan et al.* [2004]. These authors pointed out that the standard model's small-scale 3-D turbulence could destabilize any large-scale 2-D turbulence. This apparent internal contradiction offers a possible explanation for the failure to find either a k^{-3} regime or enstrophy cascade [*Strauss and Ditlevsen*, 1999] in the reanalyses. Such instability may also explain why some models such as the ECMWF forecast model apparently fail to yield $k^{-5/3}$ regimes [*Palmer*, 2001] yet at the same time, Princeton's Geophysical Fluid Dynamics Laboratory SKYHI model apparently are able to yield both $k^{-5/3}$ and k^{-3} regimes [see *Takahashi et al.*, 2006, Figure 1d; *Hamilton et al.*, 2008]. In at least some of these cases, the high wave number $k^{-5/3}$ spectral "bump" has been shown to be an artifact of the numerics due to incorrect hyperviscous "tuning" [*Smith*, 2004]. Similar claims for simultaneous $k^{-5/3}$ and k^{-3} regimes have been made for the regional WRF model [*Skamarock*, 2004], but even if the claims are valid, the k^{-3} regime is over a very narrow range and in addition, the purported $k^{-5/3}$ range is much too shallow: Figure 1e shows that in fact a single $k^{-2.4}$ regime works extremely well over the whole range.

[9] Ironically, the ability of the SKYHI or possibly the WRF models to yield two scaling regimes may not be an indication of their realism. For example, returning to Figure 1d which compares the *Takahashi et al.* [2006] Earth simulator results (6–15 day forecast) with the GASP data, we see that the scales with the largest deviations between the model and the empirical spectra (the range ≈ 400–3000 km, between the arrows) are precisely those which are supposedly explained by the existence of the two regimes! On the other hand, cascade analyses of the type described below, which neither make a priori assumptions about the physical nature of the cascade quantity nor of its isotropy or anisotropy, show that both the ERA 40 reanalyses in either space [*Stolle et al.*, 2009] or in time [*Stolle*, 2009], or meteorological models of the atmosphere (the GFS and GEM models) have nearly

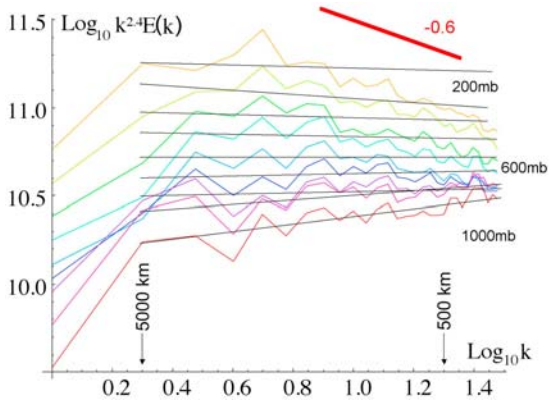

Figure 1c. The isotropic spectrum of zonal component of the wind at 200, 300, 400, …, 1000 mbar from the ECMWF interim reanalysis for January 2006 averaged between ±45° latitude. The straight lines are not regressions, rather they have the slopes of the horizontal wind in the vertical direction as estimated by drop sondes from *Lovejoy et al.* [2007]. It can be seen that the isobaric velocity spectra have exponents close to the vertical values (especially at the data-rich lower levels).

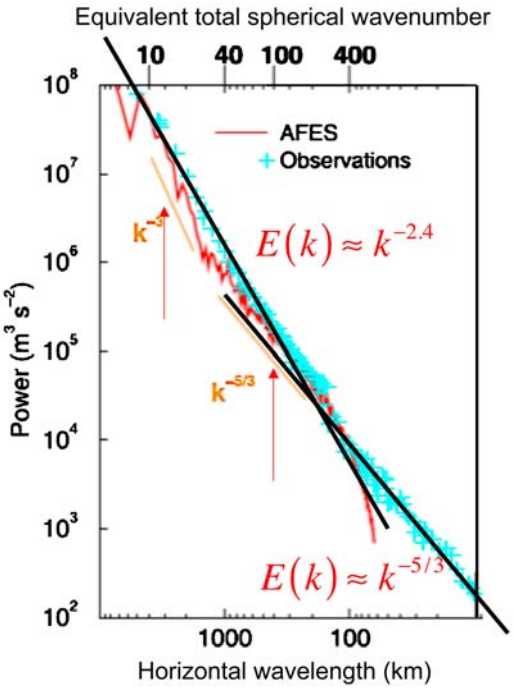

Figure 1d. The comparison of a large (T639) simulation on the Earth Simulator (zonal wind, at 45°N, 200 mbar, with forecasts for days 6–15 shown in red) with a replotting of the GASP aircraft spectra (cyan, crosses), adapted from *Takahashi et al.* [2006]. The solid black lines show the predicted isobaric and horizontal spectra that have been added for reference. It can be seen that while overall the model reproduces the GASP spectra reasonably well down to the model dissipation scales, it is striking that the largest deviations of the model from the empirical spectra are precisely in the region 400–3000 km (between the arrows) where the isobaric $k^{-2.4}$ spectrum is very accurate.

perfect scaling cascade structures over almost their entire range of spatial scales; see, e.g., Figure 1f or the numerous figures in the above references (the deviations from multiplicative cascades are between ≈ 0.5–1% up to 5000 km in scale). As argued by *Schertzer and Lovejoy* [1987] or in the review by *Lovejoy and Schertzer* [2010] the reason that this is possible (even expected), is that the models, and apparently the atmosphere, are both anisotropic but scale invariant over huge ranges. Note that boundary conditions such as the topography as well as the short- and long-wave atmospheric forcings also display scaling cascade structures over most of their observed ranges so that they are not expected to break the dynamical scaling [*Gagnon et al.*, 2006], [*Lovejoy et al.*, 2001, 2009a].

1.2. Characterizing the Horizontal Scaling of Atmospheric Fields

[10] If the atmosphere is anisotropic and scaling over wide ranges, then it is fundamentally important to characterize the anisotropic scaling regimes for as many of the fields as possible, i.e., to determine the type of scaling (including the determination of the basic turbulent exponents), as well as the limits to the scaling: the inner and outer scales. The goal of this paper is therefore to go a step beyond the reinterpretation outlined above to see how the data can be quantitatively used to characterize atmospheric turbulence while attempting to avoid spurious aircraft induced effects.

[11] The processes which account for the wide-range anisotropic scaling of the fields are the anisotropic multiplicative cascade processes, i.e., anisotropic extensions of the explicit phenomenological cascade models that were developed through the 1960s, 1970s and 1980s [*Novikov and Stewart*, 1964; *Yaglom*, 1966; *Mandelbrot*, 1974; *Schertzer and Lovejoy*, 1987]. In recent papers, we have investigated the vertical cascade structure using drop sondes [*Lovejoy et al.*, 2009b], the horizontal cascade structure using satellite data [*Lovejoy et al.*, 2009a] and vertical cross sections using lidar backscatter data [*Lilley et al.*, 2004; *Lilley et al.*, 2008]. In addition, meteorological reanalyses as well as numerical meteorological models [*Stolle et al.*, 2009; S. Lovejoy and D. Schertzer, Space-time cascades and the scaling of ECMWF reanalyses: Fluxes and fields, submitted to *Journal of Geophysical Research*, 2010] have recently been shown with high accuracy to have multiplicative cascade structures over almost their entire spatial ranges and up to about 10 days in the time domain. What is missing from a fairly complete spatial characterization of atmospheric cascades is the direct verification of the multiplicative cascade structure in the horizontal on the standard meteorological fields including the horizontal wind, the temperature, humidity, potential temperature; this is our task here.

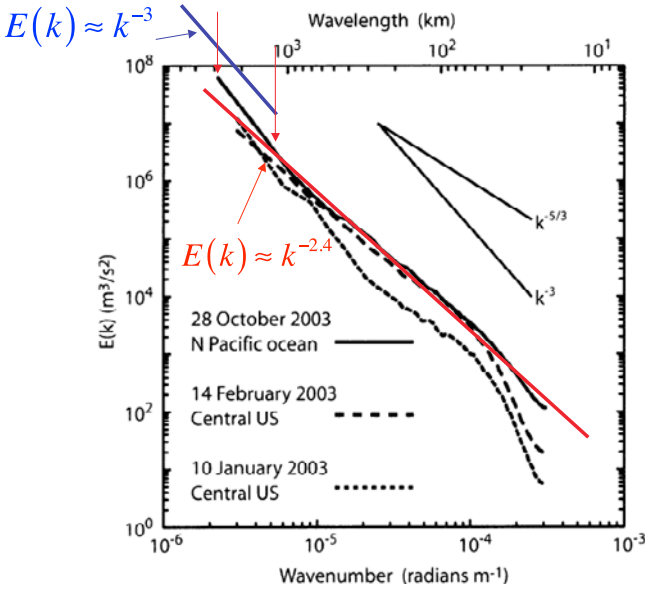

Figure 1e. Sample spectra from WRF forecasts of zonal wind averaged over the isobaric surfaces covering roughly the range 3–9 km in altitude, adapted from *Skamarock* [2004]. The claimed "clear k^{-3} regime" for the solid (oceanic) spectrum spans a range of factors 2–3 at the relatively unreliable extreme low wave numbers (between the arrows at top left). Except for the extremes, the spectra again follow the isobaric predictions $k^{-2.4}$ (red) very well over most of the range.

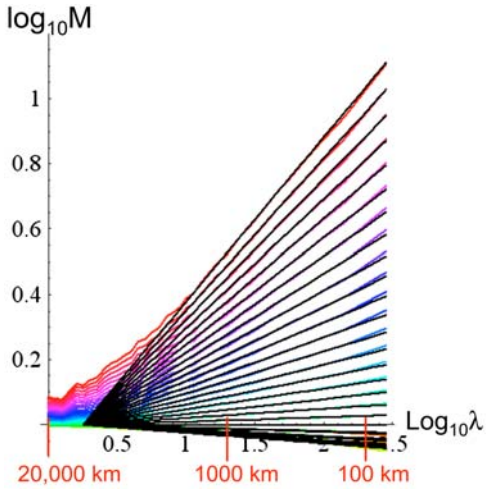

Figure 1f. The spatial scaling of the energy flux (ε) estimated from the Laplacian of the zonal wind at 1000 mbar, for the GEM model at $t = 0$ (reproduced from *Stolle et al.* [2009]; for the details of the technique, see section 2). The statistical moments M_q (equation (2)) are shown for $q = 0.0$ to 2.9 ($q > 1.0$: $\mathrm{Log}_{10}M_q > 0$, monotonically increasing; $q < 1.0$: $\mathrm{Log}_{10}M_q < 0$) in steps of 0.1, $\lambda = L_{\mathrm{earth}}/L$, $L_{\mathrm{earth}} = 20\,000$ km. The qth moment colors vary from $q = 0$ (reddish orange) to $q = 2.9$ (red). The converging straight lines show that the statistics up to order 2.9 are well approximated by a multiplicative cascade starting at about 10,000 km. The results for the GFS model are almost identical, as are the forecast fields at $t = 48$, 144 h. For scales < 5000 km the deviations from the straight lines are ≈ ± 0.6%. This may be compared with the empirical aircraft results derived in Figure 2b.

[12] This paper is structured as follows. In section 2 we review the data and discuss some of their limitations, including the connection between the wind, pressure and altitude fields, we introduce the cascade formalism. In section 3 we discuss the basic flux and fluctuation analyses of the wind, temperature, potential temperature, and humidity fields; and in section 4 we give a refined treatment attempting to determine the best regime for parameter estimation and to get the best parameter values. In section 5 we discuss outstanding issues and conclude.

2. Data: Their Intermittency

[13] The data analyzed were from the Winter Storms 2004 experiment and involved 10 aircraft flights over a roughly a 2 week period over the northern Pacific. Each flight dropped 20–30 drop sondes which were analyzed to determine the vertical cascade structure [*Lovejoy et al.*, 2009b]. For air traffic reasons, the Gulfstream 4 plane flew along either the 162, 178, or 196 mbar isobars, (to within ± 0.11 mbar; that is, the pressure level was ≈ constant to within ± 0.068%), it has a radar altimeter which is reliable over the ocean, but which is only used to anchor the GPS estimates, these geometric altitudes were used here. Each had one or more roughly constant straight and constant altitude legs more than 400 km long between 11.9, 13.7 km altitude. The data were sampled every 1 s and the mean horizontal aircraft speed with respect to the ground was 280 m/s. In addition, we checked that the distance covered on the ground between measurements was constant to within ±2% so that the horizontal velocity was nearly constant (in addition, using interpolation, we repeated the key analyses using the actual ground distance rather than the elapsed time and found only very small differences). This is the same data set analyzed by *Lovejoy et al.* [2009c] where it is described in more detail.

[14] The basic scale by scale relations between the trajectory and the fields was investigated using both spectral and cross-spectral analysis from *Lovejoy et al.* [2009c]. Figure 2a shows an extract of the latter results for simplicity showing only the results for the longitudinal (the along trajectory) component of the wind. We calculated the cross spectrum which is a kind of wave number by wave number cross-correlation coefficient. However, unlike the usual cross correlation, it is complex-valued; hence it is usual to introduce the modulus. called the "coherency" (C), and argument, the "phase" (θ) [see e.g., *Landahl and Mollo-Christensen*, 1986]. An important difference between the coherency and a cross correlation is that C is always positive; in Figure 2a, C > ≈0.2 implies a statistically significant relation. On the other hand, a positive phase in Figure 2a implies that the wind leads (pressure or altitude), a negative phase, that it lags behind. From Figure 2a we see that between about 4 and 40 km, the altitude leads the wind but the pressure lags behind: the situation is reversed at larger scales (smaller wave numbers). The direct interpretation is that for the higher wave numbers ($(4\ \mathrm{km})^{-1} > k > (40\ \mathrm{km})^{-1}$, corresponding to time scales of 10–150 s) the aircraft autopilot and inertia cause the change in altitude with the pressure then following the altitude. For the smaller wave numbers ($k < (40\ \mathrm{km})^{-1}$), the situation is reversed with the pressure changes leading (presumably causing) the change in wind and altitude; this is presumably the regime where the aircraft tightly follows the isobars.

[15] The coherency and phase analysis suggests that the main effect of the trajectory fluctuations is on the wind field and that its influence will be smaller for the other atmospheric fields (we see this below). Going beyond phases and coherencies, let us consider the detailed statistics of the trajectories. For scales less than about 4 km, the aircraft inertia smoothes them out; the main variations are smooth and are associated with various roll modes and the pilot/autopilot response. However, at scales from about 4 to 40–100 km (and from ≈3 to about 300 km for the stratospheric ER-2 trajectories along isomachs), the trajectory is fractal with the altitude lagging behind the (horizontal) wind fluctuations. Finally at scales > ≈ 40 km the aircraft follows the isobars quite closely so that the wind lags behind the pressure. These conclusions were reached by considering the average for 24 aircraft legs flying between roughly 11 and 13 km, each 1120 km long as well as through a leg by leg analysis which showed considerable variability in the scale at which these transitions occurred. According to this analysis we may anticipate that there will be a strong effect of the variability (indeed, intermittency) of the aircraft altitude on the measurements, at least for scales smaller than about 40 km where the wind leads the altitude, imposing its strong intermittency on the aircraft.

[16] In order to demonstrate this and to quantify the intermittency of the trajectory we performed a standard multifractal analysis. Since we will perform similar analyses

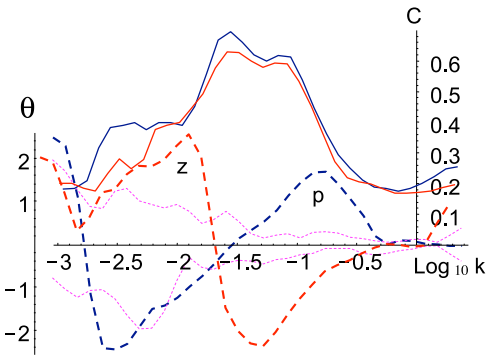

Figure 2a. Coherencies (C, right axis) and phases (θ in radians, left axis) of the longitudinal wind with pressure (blue) and altitude (red). Solid curves are coherencies; those greater than ≈0.2 are statistically significant, and they are highly significant over most of the range. Thick dashed lines are phases, and thin purple dashed lines are the 1 standard deviation confidence intervals for the phases (they increase at low wave numbers due to the smaller number of samples). A positive phase means that the wind leads (pressure or altitude); a negative phase means that it lags behind.

on the meteorological fields we give a general explanation of the method, using the example of the familiar Kolmogorov law of turbulence.

[17] Consider wind fluctuations Δv over distances Δx with underlying turbulent energy flux ε; we therefore have

$$\Delta v = \varphi \Delta x^H. \tag{1}$$

The form (1) is a generic relation between a turbulent fluctuation Δv and turbulent flux φ (at resolution Δx), the Kolmogorov law is the special case where $\varphi = \varepsilon^{1/3}$ and $H = 1/3$. Strictly speaking, the equality in equation (1) is in the sense of probability distributions; that is, the distribution of the random fluctuation Δv is the same as that of $\varphi \Delta x^H$. In the following, this distinction is not important since we use $\Delta v/\Delta x^H$ to investigate the statistical properties of φ, and equality in this weaker probabilistic sense is sufficient. In the data analyzed below, we generally took $\Delta v(\Delta x) = |v(x + \Delta x) - v(x)|$ but other definitions, such as the second finite difference rather than the first, or equivalently wavelets may be used.

[18] If over a range of scales, φ is the result of a multiplicative cascade process, then the normalized flux $\varphi_\lambda' = \varphi_\lambda / \langle \varphi \rangle$ obeys the following statistics:

$$M_q = \left(\frac{\lambda}{\lambda_{eff}}\right)^{K(q)}; \quad \lambda = \frac{L_{ref}}{L}; \quad \lambda_{eff} = \frac{L_{ref}}{L_{eff}}, \tag{2}$$

where $M_q = \langle \varphi_\lambda^q \rangle = \langle \varphi_\lambda^q \rangle / \langle \varphi \rangle^q$ is the normalized qth moment at resolution L (scale ratio λ), L_{ref} is a convenient reference scale (taken below as the largest great circle distance on the Earth, $L_{ref} = 20{,}000$ km), L_{eff} is the "effective" scale at which the cascade begins, and $K(q)$ is the scaling exponent characterizing the intermittency. Note that there is no need for a subscript on $\langle \varphi \rangle$ since the ensemble flux is a climatological value independent of the resolution λ (i.e., $K(q = 1) = 0$ which follows since for $q = 1$ the operations of spatial and ensemble averaging commute). In order to test equation (2) on the data, it is sufficient to use the (absolute) fluctuations at the smallest available scales l (i.e., take $l = \Delta x$, corresponding to the large-scale ratio Λ), and then to estimate the normalized flux as

$$\frac{\varphi_\Lambda}{\langle \varphi_\Lambda \rangle} = \frac{\Delta v(l)}{\langle \Delta v(l) \rangle}; \quad \Lambda = \frac{L}{l}. \tag{3}$$

That is, it is not necessary to know H or even the physical nature of the flux φ so that our results are independent of any specific theory of turbulence. The fluctuations can be estimated either by differences (when $0 < H < 1$) or (equivalently) by wavelets. The normalized flux at lower resolution $\lambda < \Lambda$ is then obtained by straightforward spatial averaging of the fine-scale (Λ) resolution normalized fluxes. We do not attempt to determine the direction (i.e., from large to small or small to large) of the cascade. Note that we follow standard conventions using Δx for the length scale of fluctuations and l and L for the resolutions of fluxes; Λ, λ (both ≥ 1) are dimensionless scale ratios, largest scale to inner resolution scale (Λ being the smallest available, λ can vary in the range $1 \leq \lambda \leq \Lambda$).

[19] When this method is applied to the aircraft altitude, we obtain Figure 2b which shows that equation (2) is well verified with lines converging to $\log_{10}\lambda_{eff} \approx 2.9$ corresponding to $L_{eff} \approx 30$ km. This shows that for scales $< \approx 30$ km, the altitude has very strong intermittency which is of the type theoretically predicted for turbulent cascades. This result is compatible with the phase and coherence analysis summarized above to the effect that for scales $< \approx 40$ km that the phase of the wind leads the phase of the pressure causing deviations from isobaric flight and provoking autopilot altitude compensation. While this mechanism can apparently make the altitude fluctuations lead the wind, the intermittency in the altitude due to the wind remains. At the larger scales the phase changes sign and the pressure leads the wind so that (due to the autopilot) the aircraft starts to closely follow the isobars which are much smoother (the response time of the autopilot

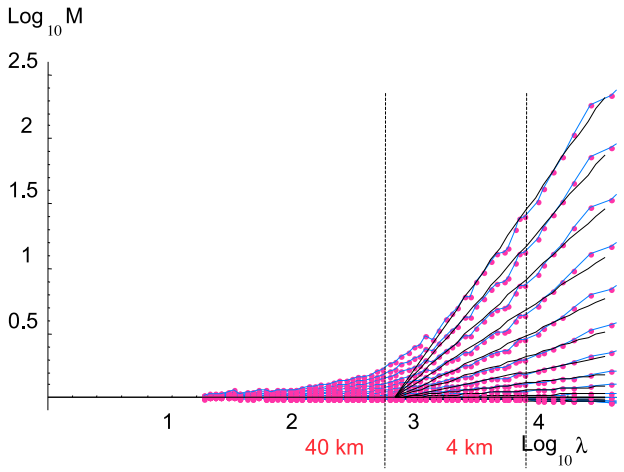

Figure 2b. The normalized moments $q = 0.2, 0.4, \ldots, 3$ for aircraft altitude z; $\log_{10}\lambda$ corresponds to 20,000 km (= L_{ref}).

Table 1. Horizontal Cascade Parameter Estimates[a]

	T	Logθ	h	v_{long}	v_{trans}	p	z
C_1	0.052	0.052	0.040	0.033	0.046	0.031	0.23
α	2.15	2.20	2.10	2.10	2.10	2.2	2.15
L_{eff} (km)	5000	10,000	10,000	10^5	25,000	1600	30
δ (%)	0.5	2.0	0.5	0.4	0.8	0.5	2.6

[a]These are estimated over the range 100 km down to 2 km except for z which is over the range 20 km to 0.5 km. The regressions force the lines to pass through a common external scale (equation (2)). L_{eff} is given in round numbers since the values were only believed to be accurate to the nearest $10^{0.1}$ i.e., to about ±25%. We have not given error estimates on the parameters because of the significant systematic (trajectory) effects. These are discussed in section 4 along with refined parameter estimates and comparisons with the reanalyses and numerical model parameters. Note that the aircraft α estimates are a bit too big since the theoretical maximum is $\alpha = 2$. They were estimated with the double trace moment technique which depends largely on the statistics of the weaker events, and these could be affected by aircraft turbulence. In our experience, values of $\alpha > 2$ are always accompanied by error bars that encompass values < 2. T, temperature; θ, potential temperature; h, humidity; v_{long} and v_{trans}, longitudinal and transverse components of the horizontal wind; p, pressure; and z, altitude of the aircraft.

is much shorter than the 2–3 min needed to cover ≈ 40 km but apparently, the turbulence is too strong at smaller scales).

[20] We now seek to quantify the accuracy with which the altitude intermittency follows the cascade form. First, we may use the logarithmic slopes of M_q to estimate $K(q)$, and then use a parametric form of $K(q)$ in order to reduce it to a manageable (finite) number of parameters. This is most conveniently done by exploiting the existence of stable, attractive cascade processes, the result of a kind of multiplicative central limit theorem, which gives rise to "universal multifractals" [*Schertzer and Lovejoy*, 1987; *Schertzer and Lovejoy*, 1997]. For universal multifractals $K(q)$ has of the form

$$K(q) = \frac{C_1}{\alpha - 1}(q^\alpha - q); \quad q \geq 0; \quad 0 \leq \alpha \leq 2. \tag{4}$$

The parameter C_1 ($0 < C_1 < D$) characterizes the intermittency of the mean: $C_1 = K'(1)$, it thus characterizes the intermittency of the mean field (D is the dimension of the observing space, here $D = 1$). The second parameter is the multifractal index α which characterizes the degree of multifractality, it quantifies how rapidly (with intensity, with q), the statistics deviate from the monofractal case $\alpha = 0$). In Table 1 we give the estimates of the parameters for the altitude and various other fields. We return in section 4 to the parameters attempting refined estimates and also comparing the values with those of reanalyses and meteorological models.

[21] To quantify the accuracy, we may characterize the deviations by the mean absolute residuals for the statistical moments M_q of order q from 0 to 2 for all points between the smallest available scale and the much larger scales indicated in the text (generally the largest possible, for a total range of 280 m to 1120 km):

$$\Delta = \overline{\left|\log_{10}(M_q) - K(q)\log_{10}(\lambda/\lambda_{eff})\right|}. \tag{5}$$

To convert Δ to a percent deviation, use $\delta = 100(10\Delta\text{-}1)$ (see Table 1 for the mean $\overline{\delta}$ averaged over the $q \leq 2$).

3. Scaling Analyses

3.1. Trace Moments and the Cascade Structure of the Fields

[22] Based on the analysis of the aircraft altitude and cross spectra, we have argued that the aircraft trajectory fluctuations and their coupling with the fields must be taken into account for quantitative analyses of the statistics. However, before we attempt a more refined analysis, we present the basic cascade (flux) and then fluctuation analyses. As indicated in section 2 (see equation (3)), the dimensionless, normalized flux is estimated using absolute fluctuations at the smallest scales. In the case of the horizontal wind in the $\approx k^{-5/3}$

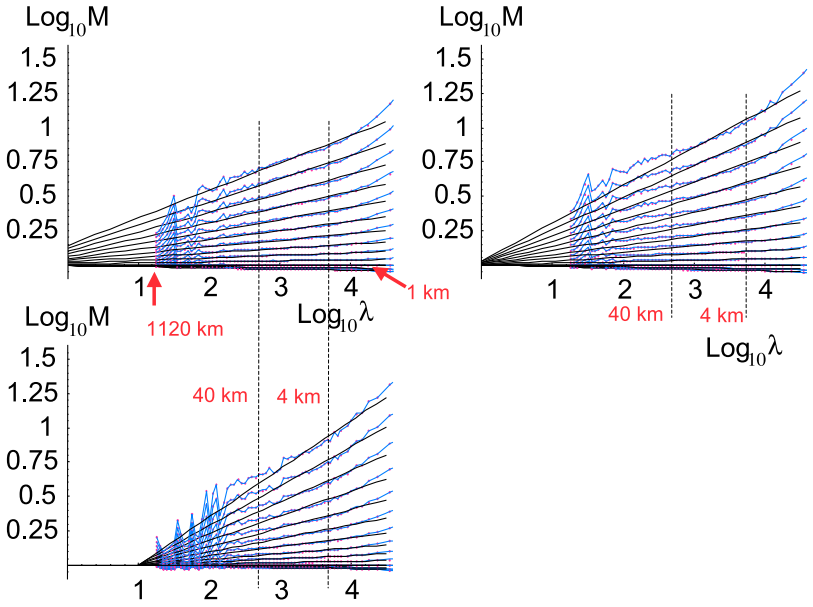

Figure 2c. Same as Figure 2b but for the fields strongly affected by the trajectories: (top left) the longitudinal wind, (top right) the transverse wind, and (bottom left) pressure.

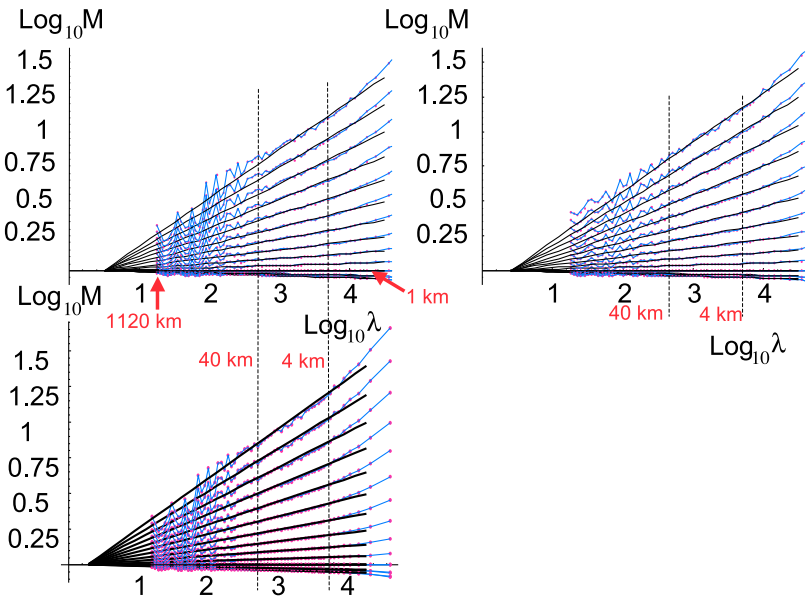

Figure 2d. Same as Figure 2c but for the fields that are relatively unaffected by the trajectory: (top left) temperature, (top right) relative humidity, and (bottom left) log potential temperature.

regime, it is presumably the energy flux to the one third power, but knowledge of the exact physical nature of the flux is not necessary to test the prediction of cascade processes (equation (2)). First we decompose the wind into longitudinal and transverse components anticipating that the altitude fluctuations will affect each somewhat differently. Figure 2c shows the results along with those of the pressure. Although the basic structure is reasonably close to (near) planetary-scale cascades, we can see evidence of the three regimes discussed above; at scales smaller than about 4 km, the variability is a little too large (compared with the regression lines), logM_q is quite linear from 4 to 40 km, and then flattens out a bit at scales > 40 km. Qualitatively this can be understood by the action of inertially smoothed trajectories at small but nonzero slopes (scales $< \approx 4$ km), by turbulent wind induced altitude fluctuations for scales between 4 and 40 km and then at larger scales an excess of variability since the aircraft starts to follow the isobaric slopes and responds to the (larger) vertical intermittency (at 40 km the statistics are still quite good and we see a systematic departure above the regression lines, not just noise). For the pressure, on the contrary the variability at the largest scales is low since the aircraft does not stray far from the isobars. We may also note that for the wind, the outer scales are somewhat larger than the planetary scales (Table 1), especially for the longitudinal component. *Lovejoy et al.* [2009c] have already argued on the basis of cross-spectral analysis that the longitudinal component was the most affected by the trajectory; it is presumably partially responsible for the corresponding large value of L_{eff} which implies an excessively large variability at all scales. In comparison, the value of L_{eff} for the transverse component, although perhaps still too large, is about the same as that reported for satellite radar reflectivities from precipitation [*Lovejoy et al.*, 2008a]; the fact that it is larger than the largest great circle distance (20,000 km) simply means that even at planetary scales there is residual variability due to the interactions of the wind with other atmospheric fields. In comparison the outer scale of the pressure is somewhat smaller than planetary scales; this is not surprising since the aircraft was attempting to fly along isobars.

[23] Turning our attention to the analyses of the relatively unbiased temperature, humidity and log potential temperature fields (Figure 2d), we again see evidence for the three regimes and we note that the cascade structure is somewhat more closely followed with external scales somewhat smaller than 20,000 km. Overall, we conclude that the basic predictions of the cascade theories are well respected; in particular there is no evidence for a break anywhere near the mesoscale ($\approx$ 10 km, no sign of a 2-D/3-D transition). The outer scales of these fields are in fact very close to those of visible, infrared and passive microwave radiances as determined by satellite [*Lovejoy et al.*, 2009a]. Note that the log equivalent potential temperature is not shown here or below because the humidity is sufficiently low at the aircraft altitude that the graph is nearly indistinguishable from that of the log potential temperature.

3.2. Fluctuation Analysis Using Structure Functions

[24] In section 3.1 we discussed the statistics of the turbulent flux, we now turn our attention to the (absolute) fluctuations as functions of scale (Δx), here estimated using differences: e.g., $\Delta v(\Delta x) = |v(x + \Delta x) - v(x)|$. Defining the qth-order structure function (S_q),

$$S_q(\Delta x) = \langle \Delta v(\Delta x)^q \rangle, \tag{6a}$$

we can now take the ensemble average of equation (1) and obtain

$$S_q(\Delta x) \propto \Delta x^{\xi(q)}; \quad \xi(q) = qH - K(q). \tag{6b}$$

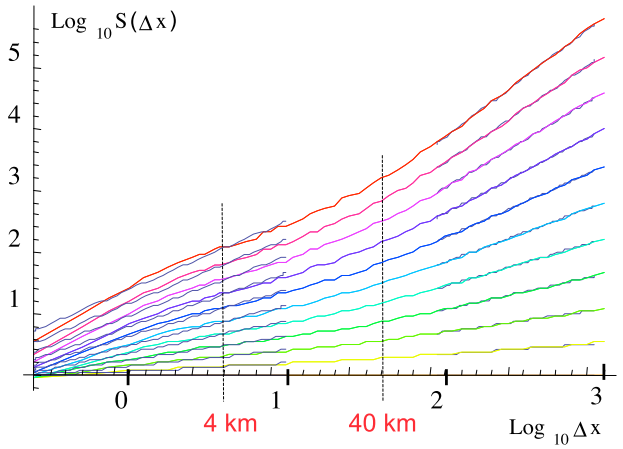

Figure 3a. Structure functions of order $q = 0.2, 0.4, \ldots, 2.0$ for the aircraft altitude (bottom to top). Distances Δx are in kilometers. Separate sets of regression lines are shown for both small and large scales in order to emphasize the change with scale.

The difference between the structure function and the fluxes can be clearly seen in the special case of 1-D analyses where fluxes at the smallest scale are estimated by absolute first-order differences (as described in section 2). In this case, the large-scale fluxes are obtained by adding/integrating the absolute small-scale differences. In the case of structure functions, the large-scale fluctuation is given by adding/integrating the signed small-scale differences. In terms of scaling, the former yields an exponent $K(q)$ (with respect to λ) while the latter has exponent $Hq - K(q)$ (with respect to $\Delta x = L_{outer}/\lambda$). Since the linear term Hq is frequently larger than the nonlinear term $K(q)$ (associated with intermittency) studying the fluxes is a more sensitive way of investigating the cascade, intermittency behavior.

[25] The results for altitude are given in Figure 3a. We again see evidence for three regimes; the large-scale regime very nearly corresponds to linear variations ($H = 1$), i.e., to a constant slope with the aircraft nearly exactly following the isobars. As we shall see in more detail in the section 4, where we estimate H as a function of scale from the logarithmic slopes of Figure 3a, H decreases at the smallest scale from a value ≈ 1 corresponding to inertially smoothed trajectories, to a minimum value ≈ 0.5 at around 4 km, and then increases to the maximum value 1 for scales > 40 km where the trajectories are close to isobars and are again, relatively smooth. Note that in Figures 3a, 3b, and 3c we plot the nondimensional structure functions obtained by dividing the fluctuations by the mean at the smallest scale.

[26] In Figure 3b we show the corresponding results for the longitudinal and transverse wind and pressure. While the behavior for the wind has essentially two scaling regimes with a 4–40 km transition regime, unsurprisingly, the pressure has poor scaling; we reserve a detailed analysis for section 4. In Figure 3c we show the corresponding plot for those fields less affected by the trajectory fluctuations, the temperature, humidity and log potential temperature; we see that the scaling is indeed very good.

4. Refined Analysis

4.1. Horizontal Exponent Estimates

4.1.1. Intermittency Exponents and the Optimum Scale Range

[27] In section 3 we considered the raw flux statistics; no attempt was made to quantitatively correct or take into account the effects of the trajectory, we turn to this task now. From the "raw" flux and fluctuation analyses, we saw that the

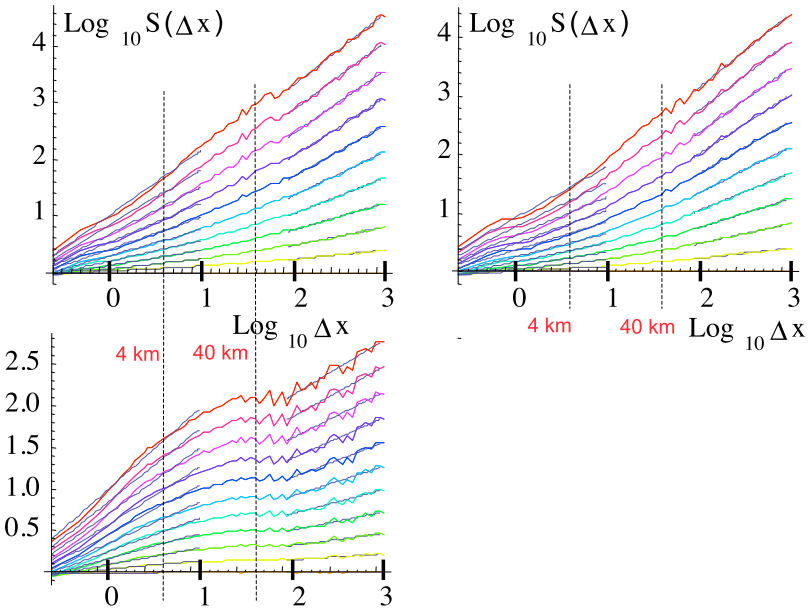

Figure 3b. Same as Figure 3a a but for the fields strongly affected by the aircraft trajectory: (top left) the longitudinal wind, (top right) the transverse wind, and (bottom left) the pressure.

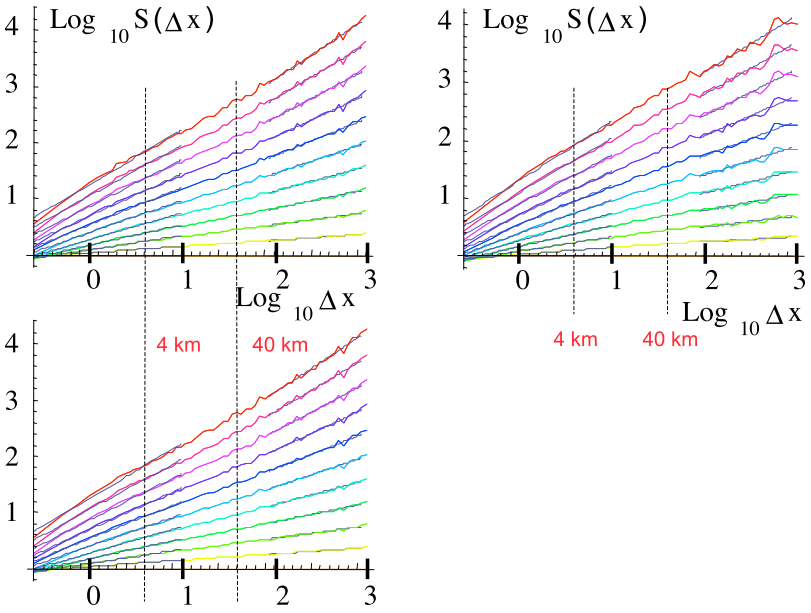

Figure 3c. Same as Figure 3a but for those fields relatively unaffected by the aircraft trajectories: (top left) the temperature, (top right) the humidity, and (bottom left) the log potential temperature.

aircraft trajectories are highly intermittent for scales < 40 km (Figure 2a) after which they begin to accurately follow isobars and have nearly constant slopes (Figure 2b). We also saw that for the fields not strongly affected by the trajectory (temperature, humidity, log potential temperature), that the overall scaling was very good. However, if we want to quantitatively characterize the corresponding horizontal scaling and estimate $K(q)$ and hence the parameters H, C_1, α, it is not clear what is the optimum range of scales that should be used. In order to obtain a more exact picture of the scale by scale variations in the statistics, we first consider scale by scale estimates of the basic flux and intermittency parameters using the logarithmic derivatives of the second-order flux exponent ($K(2)$) and first-order ($q = 1$) structure function exponent H. $K(2)$ was chosen to characterize the amplitude of the intermittency rather than the more fundamental C_1 because it is directly related to the spectral exponent $\beta = 1 + 2H - K(2)$ and so can be directly used to determine the contribution of intermittency corrections to the spectrum (note that since $\alpha \approx 2$ we have $C_1 \approx K(2)/2$ (equation (4)); in any case, C_1 is directly estimated below using $C_1 = K'(1)$).

[28] Figure 4a shows the results for the second moment of the flux M_2; Figure 4a (right) for the moments themselves, Figure 4a (left) for the corresponding logarithmic derivatives estimated from the corresponding right hand graphs by performing regressions over an octave of scales centered on the scale indicated. Focusing on Figure 4a (top) for the wind, we see that the logarithmic derivatives bring out the three regions quite clearly. At small scales $< \approx 4$ km (large λ), the intermittency is large corresponding to the strong intermittency of the trajectory while at the largest scales $> \approx 40$ km (small λ) it is again large due to the fact that the near constant slope means that the aircraft is picking up the (large) vertical intermittency indeed, if we use the vertical value $K(2) \approx 0.17$ estimated from the drop sondes we find that it is not far from the value of the top left (velocity) graph in Figure 4a. Note that the estimate of the logarithmic slope is itself highly fluctuating at low λ since the statistics get progressively worse at large scales due to the smaller and smaller number of large-scale structures. Detailed consideration of the scale by scale estimates of $K(2)$ for the altitude show that it is actually not so constant in spite of the relatively straight appearance of the lines in Figure 2a. For the velocity, the region 4–40 km is the least intermittent (in the sense of the lowest exponent $K(2)$); this is presumably the optimum region for estimating the scaling exponents: at smaller scales, the aircraft trajectory is too intermittent whereas at the larger scales, the intermittency increases again since, at least for the wind, the aircraft is moving significantly in the vertical along a near constant isobaric slope (in any case at the large scales, we obtain the vertical rather than the horizontal exponents and the vertical intermittency is larger; see below and Figure 2c). We therefore used this regime to estimate the exponents (Table 2 shows the estimates obtained by taking regression over the range 4–40 km). We see that in conformity with the cross-spectral analyses and our previous discussion, that the scale by scale intermittency (i.e., $K(2) = dlogM_q/dlog\lambda$) for T, $\log\theta$ and h is nearly constant for scales $> \approx 4$ km confirming that the main deviation from scaling for these fields is only at the smallest scales. We also observe that the exponents are nearly the same for all three fields. In Table 2 we also give the corresponding C_1 estimates obtained by numerically estimating $K'(1)$ using regressions over the range 4–40 km.

4.1.2. Fluctuation Exponent H

[29] Turning our attention to the fluctuation exponent H (Figure 4b, top right; see the reference lines), we see that they reasonably follow successively the values $H = 1/3$, 0.75 (i.e., the standard Kolmogorov value and the observed vertical value, respectively). However, the scale by scale estimates (Figure 4b, top left) show that this mean behavior hides an

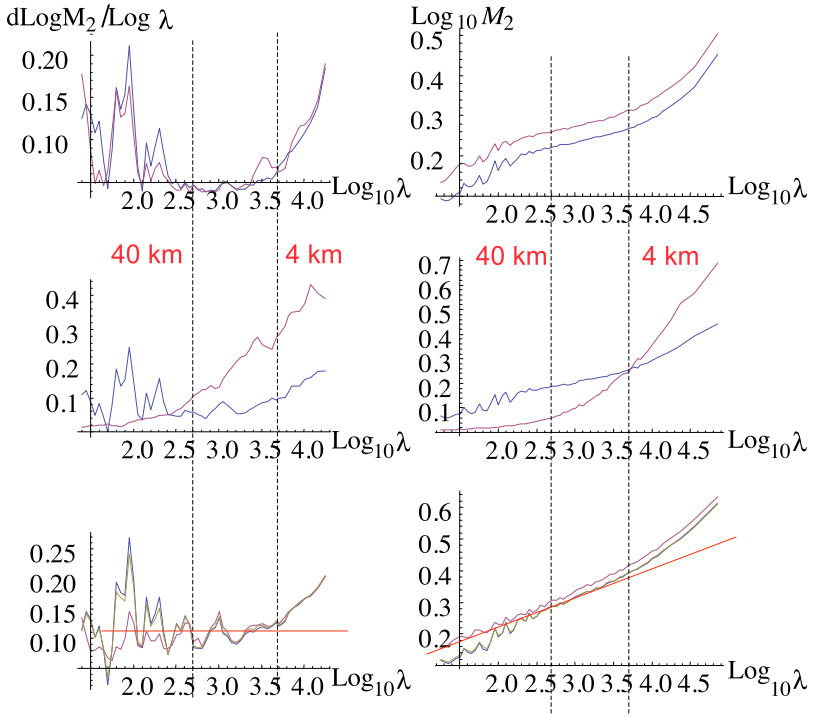

Figure 4a. (right) Second-order trace moments and (left) their logarithmic derivatives (estimates of $K(2)$, an intermittency index). (top) Wind, longitudinal (blue) and transverse (red). The region within the dashed lines has particularly low $K(2)$ (≈ 0.05). (middle) Pressure (blue) and altitude (red). (bottom) Temperature (blue), humidity (red), and log potential temperature (gold); reference lines $K(2) = 0.12$. $\text{Log}_{10}\lambda = 0$ corresponds to 20,000 km ($= L_{\text{ref}}$).

increase in H from ≈ 1/3 at the smallest scales to $H \approx 0.75$ at scales 40–100 km. According to the leg by leg analyses by *Lovejoy et al.* [2009c], this fairly systematic increase of ensemble mean H hides highly variable transition scales in individual legs; the observed fairly continuous change in H is in fact the result of the transition scale varying greatly from leg to leg. On the structure function (Figure 4b, top right) we can also see that fitting a single line through the entire range is not so bad, and yields roughly the mean of 1/3 and 0.75; this may explain the wind value $H \approx 0.56 \pm 0.02$ from S. J. Hovde et al. (Vertical scaling of the atmosphere: Dropsondes from 13 km to the surface, submitted to *Nonlinear Processes in Geophysics*, 2010) (using nearly the same data set as here). This can be compared to the stratospheric estimates over (different) fractal isomach trajectories of 0.50 ± 0.02, 0.52 ± 0.03 (transverse and longitudinal wind, respectively [*Lovejoy et al.*, 2004]) and 0.53 ± 0.01 [*Tuck et al.*, 2004]. Note that the latter finds significant differences in H for the wind for stratospheric trajectories across or along the polar jet (0.45 ± 0.14 and 0.55 ± 0.12, respectively) but this could be a reflection of a systematic shift in the transition scale from an $H \approx 1/3$ to an $H \approx 0.75$ regime (see however the interpretation by *Tuck et al.* [2004] and *Tuck* [2008], which is consistent with the thermal wind equation).

[30] Moving down Figure 4b (middle), we see that at small enough scales, the altitude has $H_{tr} \approx 1$ presumably as a consequence of the inertial smoothing leading to near linear behavior (nearly constant slopes; the subscript "tr" is for "trajectory"). At larger scales, the inertia effect is gradually overcome by turbulence so that at 4 km it reaches a minimum near $H_{tr} \approx 0.48$ after which it systematically rises again to the smooth trajectory $H_{tr} \approx 1$ (for scales > ≈ 40 km) as the aircraft flies increasingly close to a constant isobaric slope. Up to this scale, the altitude statistics are thus close to those of the ER-2 stratospheric trajectories except that the latter maintain a value $H_{tr} \approx 0.58$ along isomachs (over the range ≈ 3 km until ≈ 300 km when the systematic vertical rise of ≈ 1 m/km (due to fuel consumption) eventually implies $H_{tr} \approx 1$ (on average, for scales > ≈ 300 km [*Lovejoy et al.*, 2004]). As noted above, along this fairly wide fractal range, the ER-2 had an "anomalous" wind exponent $H_{\text{wind}} \approx 0.5$ which is nearly the mean of the horizontal and vertical values (1/3, 0.75) so that the effect of following a fractal trajectory with fairly well defined fractal dimension ($= 1 + H_{tr}$) apparently leads the ER2

Table 2. Parameter Estimates Over the Optimum Range 4–40 km[a]

	T	$\log\theta$	h
α	1.78	1.82	1.81
β	1.89	1.91	1.99
$K(2)$	0.12	0.12	0.11
C_1	0.064	0.063	0.051
$C_{1,\text{st}}$	0.040	0.042	0.028
$C_{1\text{mean}}$	0.052 ± 0.012	0.052 ± 0.010	0.040 ± 0.012
H_{st}	0.49	0.50	0.52
H_β	0.51	0.52	0.50
H_{mean}	0.50 ± 0.01	0.51 ± 0.01	0.51 ± 0.01

[a]Here β is the spectral exponent, $H_{st} = \chi(1)$ is estimated from the first-order structure function, $H_\beta = (\beta + K(2) - 1)/2$, and H_{mean} is the average of the two. $C_1 = K'(1)$ from the trace moments, and $C_{1,\text{st}} = \xi(1) - \xi'(1)$; $C_{1\text{mean}}$ is the average. T, temperature; θ, potential temperature; h, humidity.

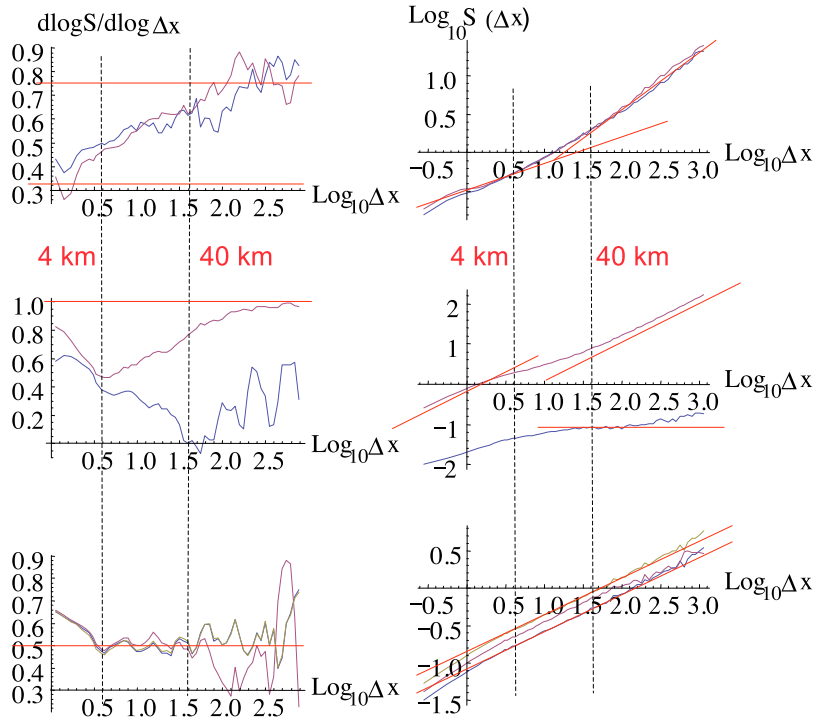

Figure 4b. (right) First-order structure functions and (left) their logarithmic derivatives (estimates of H). (top) Wind, longitudinal (blue) and transverse (red); the reference lines correspond to the exponents 1/3 and 0.75. (middle) Pressure (blue) and altitude (red); the reference lines correspond to $H = 1$, i.e., constant mean slopes. (bottom) Temperature (blue), humidity (red), and log potential temperature (gold); reference lines $H = 0.5$.

to sample both horizontal and vertical exponents yielding overall an average of the two.

[31] Consider now the pressure exponent. At the smallest scales, it starts off with a value near 2/3 decreasing systematically to zero at scales $> \approx 40$ km indicating very low fluctuations consistent with near isobaric trajectories (there are some large fluctuations in the scale by scale estimates presumably due to poor statistics). The small-scale value $\approx$ 2/3 is presumably a consequence of the dynamic pressure relation $\Delta p \approx \rho \Delta v^2/2$ so that $H_{\text{press}} = 2H_{\text{wind}}$ with $H_{\text{wind}} \approx 1/3$.

[32] Finally, in Figure 4b (bottom), we show H estimates for T, $\log\theta$, h, again finding relatively good scaling (constant exponents) for scales $> \approx 4$ km with $H \approx 0.50$ for all three (see Table 2). For temperature, this is also close to the value 0.52 ± 0.02 obtained from the similar tropospheric data (Hovde et al., submitted manuscript, 2010) and also not far from stratospheric ER-2 analyses with $H_{\text{temp}} \approx 0.45 \pm 0.02$ [*Lovejoy et al.*, 2004], and $H_{\text{temp}} \approx 0.54 \pm 0.01$ [*Tuck et al.*, 2004]. This value is so close to a ratio of small integers (1/2) that one would expect there to be a straightforward theoretical explanation (or at least dimensional analysis) leading to this value but we are not aware of any adequate theory. The usual argument is to consider temperature to be a passive scalar in which case Corrsin-Obukhov theory predicts $H = 1/3$ (see *Tuck* [2008] for arguments about the nature of atmospheric temperature that imply it is not a passive scalar). Alternatively, consider the prediction of Bolgiano-Obkuhov theory for isotropic buoyancy driven turbulence, which for the wind predicts $H = 3/5$ which, recalling $\beta = 1 + 2H - K(2)$ with K(2) $\approx$0.05, is the vertical value observed near the surface ($\approx$2.15, see section 1.1). However, the same theory predicts $H_{\text{temp}} = 1/5$ which is even further from the empirical value [see *Monin and Yaglom*, 1975]. Further support for the non standard value $H \approx 1/2$ for temperature (corresponding to $\beta \approx$ 1.9) comes from aircraft temperature spectra in the lower troposphere [*Chigirinskaya et al.*, 1994] where $\beta \approx 1.9$ fits very well over the range > 1 km in scale, and stratospheric potential temperature spectra where $\beta \approx 1.9$ is also very close to data for scales $> \approx$3 km in scale [*Bacmeister et al.*, 1996] (recall that $K(2) \approx 0.1$ so that $\beta = 1 + 2 \times 0.5 - 0.1 = 1.9$).

4.1.3. Spectral Exponent β

[33] Finally, we consider the spectra (Figure 4c). As indicated above, since the spectrum is a second-order statistic, we expect that the scale by scale analysis of the latter (again by logarithmic derivatives) should at least roughly satisfy the equation $\beta = 1 + 2H - K(2)$ (actually, this equation is strictly only valid when the scaling is satisfied over wide ranges so hence some deviations are to be expected; note that to estimate the spectrum, we used a standard Hanning window). Starting with the wind (Figure 4c, top), we see the spectral version of the transition discussed earlier: at low wave numbers ($k < (40\text{ km})^{-1}$), $\beta \approx 2.4$ ($= 2 \times 0.75 - 0.1$) to $\beta \approx$ 1.6 ($= 2 \times 1/3 - 0.05$ for $(40\text{ km})^{-1} > k > (4\text{ km})^{-1}$). In the high wave number regime, we see a new feature which is a slight bump near $k \approx (1\text{ km})^{-1}$, (magnified in the derivative on the left) which may be a residual signature of various aircraft roll modes and autopilot feedbacks. Turning our attention to Figure 4c (middle) (altitude, pressure), we see that the small

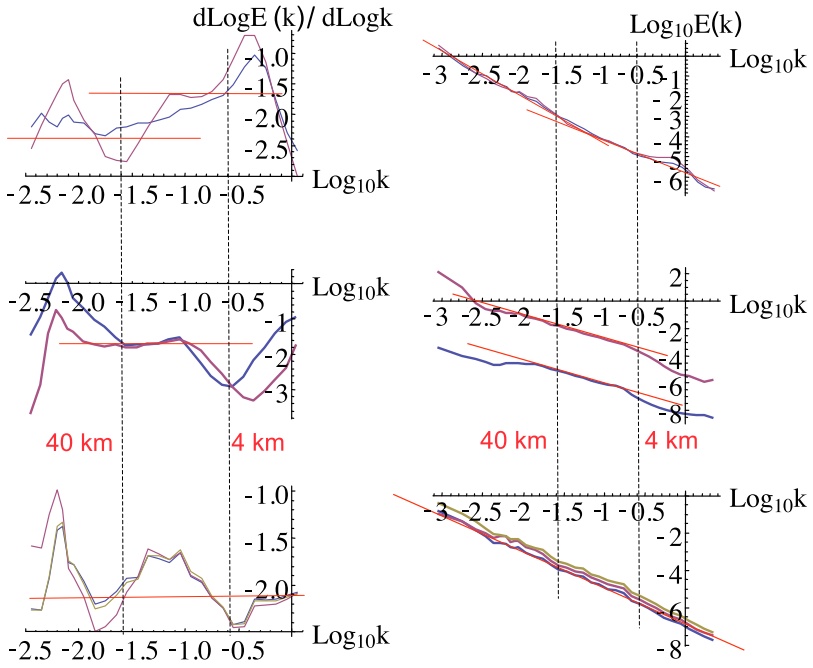

Figure 4c. (right) Spectra and (left) their logarithmic derivatives (estimates of $-\beta$). (top) Wind, longitudinal (blue) and transverse (red). The thin reference lines correspond to $\beta = 5/3, 2.4$. (middle) Pressure (blue) and altitude (red), with reference lines corresponding to $\beta = 5/3$. (bottom) Temperature (blue), humidity (red), and log potential temperature (gold); reference lines $\beta = 2$. Vertical dashed lines indicate the region with scales 4–40 km where the velocity intermittency is low.

scales are indeed particularly smooth with the larger scales following near Kolmogorov ($\beta \approx 5/3$) behaviors (probably the maximum near $(200\ \text{km})^{-1}$ is only a statistical fluctuation). Interestingly, the regime with reasonable $\beta \approx 5/3$ scaling seems to be a consequence of the partial cancellation of a continuously varying H and $K(2)$ (compare the corresponding plots of Figures 3a and 3b). Finally, the temperature, humidity and log potential temperature (Figure 4c, bottom) are seen to have significant fluctuations (Figure 4c, bottom left), but the overall scaling (to the right of Figure 4c, bottom right) is nevertheless fairly good.

[34] We now consider the parameter estimates (Table 2), taken from the "optimum" regime 4–40 km. For both the C_1 and H, there are two slightly different ways to estimate them. H can be estimated from both structure functions: $H_{st} = \xi(1)$ and also from the spectral exponent β via: $H_\beta = (\beta - 1 + K(2))/2$. The C_1 can be estimated from the flux moments: $C_1 = K'(1)$ and also from the structure function exponent: $C_1 = \xi(1) - \xi'(1)$. In Table 2 we have given all these estimates as well as the mean of the two as the best guess, and with the error as half the difference. From Table 2 we see that the three fields have nearly identical exponents, and that the important parameter H, which should ultimately be determinable by dimensional analysis, is near the value 1/2.

[35] In Figure 5 we show the moment scaling exponents $K(q)$ estimated over the 4–40 km range. We see that T, $\log\theta$, h remain almost indistinguishable out to very large q values (corresponding to rare extreme fluxes) whereas the longitudinal and transverse components separate for $q > \approx 3$ (already a large value of q). The corresponding asymptotic linearity is predicted as a consequence of a "multifractal phase transition" [*Szépfalusy et al.*, 1987; *Schertzer et al.*, 1993] and depends on the finite size of the sample (the asymptotic slope is simply the largest singularity present in the sample).

4.2. Comparison With Reanalyses and Numerical Models

[36] In section 1 we mentioned that the same basic horizontal cascade structure was found in reanalyses and in numerical models of the atmosphere (see the example in

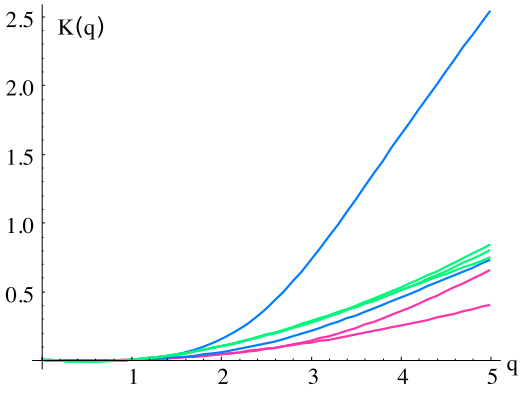

Figure 5. The $K(q)$ functions for altitude and pressure (upper and lower blue curves, respectively), temperature, humidity, and log potential temperature (lower, middle, and upper green curves, respectively), and longitudinal and transverse wind (upper and lower red curves, respectively).

Table 3. Optimum Parameters at the 200 mbar Level for the Temperature, Zonal Wind, and Humidity for the Analysis of the ERA40, GFS, and GEM Reanalysis Models[a]

	C_1	α	$L_{\rm eff}$	δ
***T* (200 mbar)**	**0.075 ± 0.05**	**1.89 ± 0.04**	**10500 ± 2000**	**0.6**
T (aircraft)	(0.107), 0.056	1.78	5000	0.5
***U* (200 mbar)**	**0.078 ± 0.006**	**1.88 ± 0.03**	**13700 ± 4000**	**0.4**
U (aircraft)	(0.088), 0.040	1.94	25000	0.8
***H* (200 mbar)**	**0.098 ± 0.012**	**1.66 ± 0.10**	**25000**	**0.6**
h (aircraft)	(0.083), 0.040	1.81	10000	0.5

[a]The 200 mbar level is roughly the aircraft altitude (boldfaced entries). ERA40, GFS, and GEM reanalysis models are estimated over a scale range starting from the model hyperdissipation scales up to 5000 km (taken from Table 2 of *Stolle et al.* [2009]). The principle value is the mean and the plus/minus indicates the spread about the mean. For *h* (200 mbar) the model values for $L_{\rm eff}$ were 10,000 (GFS), 33,000 (GEM), and 50,000 (ERA40), so that the geometric mean but no spread is given. For the C_1 aircraft estimates, the second value is from Table 2; the first (in parentheses) is the same but increased by the factor 2.08 as a rough attempt to correct for the difference in the fluxes estimated in the scaling and dissipation regimes. C_1 is the codimension of the mean characterizing the sparseness of the intensity level which gives the dominant contribution to the mean, α characterizes the degree of multifractality, $L_{\rm eff}$ is the effective outer scale of the cascade, and δ is the percentage deviation from the theoretically predicted cascade form.

Figure 1e and *Stolle et al.* [2009]). It is therefore of interest to compare the cascade parameters with those found for the aircraft data studied here. Before doing so, it should be mentioned that the turbulent fluxes estimated for the spatial cascade analyses are based not on scaling range estimates (as here; see equation (1)) but rather on the model (hyper) dissipation scale estimates (using absolute numerical Laplacians). As pointed out by *Stolle et al.* [2009], the fluxes estimated in the two different ways will in general be different. In the simplest case, assuming the standard turbulence results for the velocity field with $k^{-5/3}$ horizontal spectrum, the two fluxes are related by a power law (exponent $\eta = 3/2$). For universal multifractal cascades, this implies that the C_1 parameters are estimated by $C_{1\rm diss}/C_{1\rm scaling} = (\eta)^{\alpha}$, and with $\alpha \approx 1.8$, we find a ratio ≈ 2.08 in this basic intermittency parameter (the parameter α should be the same). Although in general the relation between the fluxes and the parameters will be more complex, the ratio 2.08 turns out to be reasonable estimate.

[37] In Table 3, we compare the best aircraft and model estimates. Overall, we see that there is surprisingly close agreement.

4.3. Horizontal-Vertical Comparison, Vertical Stratification, and Estimating H_z and $D_{\rm el}$

[38] We have argued that atmospheric fields are compatible with wide-range horizontal scaling and have estimated the corresponding exponents. This work complements that of *Lovejoy et al.* [2009b] where high-resolution drop sondes were used to estimate the corresponding vertical cascades and exponents; the overall conclusion is thus that the dynamics are scaling and turbulent but anisotropic. The simplest anisotropic turbulence model involves a unique scale function for all the fields. This would imply that the ratio of horizontal and vertical components is $H_{\rm hor}/H_{\rm ver} = H_z =$ constant, so that for universal multifractals $\alpha_{\rm hor} = \alpha_{\rm ver}$ and $C_{1\rm hor}/C_{1\rm ver} = H_z$. *Lilley et al.* [2008] provided an extensive analysis of this for the lidar backscatter data (*B*) from passive pollutants. Recall that the significance of H_z is that it controls the scaling of the aspect ratio of structures in vertical sections. In particular, if we assume horizontal isotropy, then volumes of structures vary as L^{2+Hz} where L is their horizontal extent, hence the "elliptical dimension" $D_{\rm el}$ controlling the rate of change of volumes of nonintermittent structures is $D_{\rm el} = 2 + H_z$. The 23/9 D model derives its name from $H_z = 5/9$, the result of Kolmogorov scaling ($H = 1/3$) in the horizontal and Bolgiano-Obukhov scaling in the vertical ($H = 3/5$). In comparison, the popular quasi-linear gravity wave theories [*Gardner*, 1994; *Dewan*, 1997] have $H = 1/3$ in the horizontal and $H = 1$ in the vertical so that $H_z = 1/3$ and $D_{\rm el} = 7/3$.

[39] Combining the results from the aircraft and the drop sondes and taking into account a small apparent altitude dependence of the sonde intermittency exponents C_1 (so as estimate them at the 200 mbar aircraft level), we obtain Table 4. Note that the value for the horizontal wind is given as the theoretical value 1/3 whereas the detailed leg by leg analysis by *Lovejoy et al.* [2009c], which fits two power laws (one for small, the other for large scales), gives 0.26 ± 0.07, 0.27 ± 0.13 for the dominant small-scale exponent (transverse and longitudinal, respectively). Given the strong coupling between the aircraft trajectory and the wind, it seemed best to assume that these estimates support the Kolmogorov value 1/3 and it was used without an error bar. Similarly, the value of H_z for velocity is from the analysis of *Lovejoy et al.* [2009c] which fits two power laws, one fixed at $H_h = 1/3$, the other (large-scale one corresponding to H_v) varying.

[40] It should be noted that although in Table 4 we give the ratio of the C_1 values, since their values are small, their relative errors are large and consequently their ratios have large

Table 4. An Intercomparison of Multifractal Parameters in the Horizontal and Vertical Directions[a]

	T	Logθ	*h*	*v*	*B*
α_h	*1.78*	1.82	1.81	1.94	1.83
α_v	1.70	1.90	1.85	1.90	1.82
H_h	0.50 ± 0.01	0.51 ± 0.01	0.51 ± 0.01	1/3	0.33 ± 0.02
H_v	1.07 ± 0.18	1.07 ± 0.18	0.78 ± 0.07	0.75 ± 0.05	0.60 ± 0.02
$H_z = H_h/H_v$	0.47 ± 0.09	0.47 ± 0.09	0.65 ± 0.06	0.46 ± 0.05	0.55 ± 0.02
$C_{1\rm h}$	0.052 ± 0.012	0.052 ± 0.010	0.040 ± 0.012	0.04	0.076
C_{1v}	0.072	0.071	0.091	0.088	0.11
$H_z = C_{1\rm h}/C_{1\rm v}$	0.72	0.71	0.44	0.45	0.69 ± 0.2

[a]Used is the estimate of the vertical H_v, $C_{1\rm v}$ from sondes [*Lovejoy et al.*, 2009b, Table 2]. The (horizontal) values for H_h for *T*, logθ, *h* are from Table 2 (from 4 to 40 km; see section 4.1), for the lidar reflectivity *B* it is from *Lilley et al.* [2008]. Finally, the C_1 for *v* is for the range 4–40 km using trace moments. The horizontal α values were for nonlinear fits of the $K(q)$ for $0 < q < 3$ (same range of scales). *T*, temperature; θ, potential temperature; *h*, humidity; and *v*, longitudinal component of the horizontal wind.

uncertainties. Since the H are larger, the ratio $H_z = H_h/H_v$ is more reliable than C_{1h}/C_{1v}; indeed in the latter case the error is very hard to reliably estimate and is not indicated except in the lidar case. The main conclusions are (1) for T, $\log\theta$ and v, the exponent ratio H_z is close to 0.47, (2) for T, $\log\theta$, B, and H_z it is within 1 standard deviation of the 23/9 D model value $H_z = (1/3)/(3/5) = 5/9$, and (3) the value for the humidity is somewhat larger. Note that finding virtually identical exponents for T and $\log\theta$ is not surprising since if the pressure is exactly constant, then the two have a one to one (albeit nonlinear) relation. Finally, also using the Gulfstream 4 data, Hovde et al. (submitted manuscript, 2010) find $H = 0.45 \pm 0.03$ for the humidity (see also *Tuck* [2008] for a possible explanation for the low value).

[41] If the ratios in Table 4 are taken at face value then we are led to the conclusion that two or possibly three scale functions are required to specify the scale of atmospheric structures. While this is certainly possible, let us for the moment underline the various difficulties in obtaining the in situ estimates: the nontrivial vertical dropsonde outages and the nontrivial aircraft trajectory fluctuations. In addition, recall that detailed analysis of the altitude dependence of the horizontal velocity exponent by *Lovejoy et al.* [2007] indicates that starting with the theoretical Boligano-Obukhov value 3/5 near the surface, the exponent increases somewhat with altitude to the value ≈ 0.75 at 10–12 km. Similarly, the humidity (and hence $\log\theta_E$) exponents may have both horizontal and vertical variations which may account for their high H_z values (recall however that the values of H are expected to be determined by dimensional analysis on fluxes; they are not expected to have truly continuous variations). We should therefore regard these studies as only early attempts to quantify the stratification.

5. Conclusions

[42] Satellites and other remote methods make the determination of the scale by scale statistical properties of atmospheric radiances relatively easy to establish. In comparison, our knowledge of the corresponding variability of the standard atmospheric fields (wind, temperature, humidity, etc.) is quite meager and is based almost entirely on problematic in situ measurements. The fact that today's in situ atmospheric data are often orders of magnitude better than those available even 20 years ago, and are often easily accessible, has unfortunately encouraged naïve applications. For example, in a series of papers, we have argued that the extreme (and highly clustered) nature of data outages in drop sonde profiles must be carefully taken into consideration when they are analyzed [*Lovejoy et al.*, 2009b]. In situ aircraft data provide another relevant example: not only do aircraft now have about 10 times higher resolution than they did in the 1980s (e.g., 3 km for GASP, 280 m for the Gulfstream 4), more importantly, their altitude data are sufficiently accurate so as to permit a quantitative study of the relation between the aircraft altitude, pressure and turbulence. In a related paper, we used this information to argue that due to strong coupling over wide ranges of scale between the wind and the trajectories, that aircraft measurements require a theory of anisotropic scaling turbulence for their interpretation [*Lovejoy et al.*, 2009c]. Whereas the classical interpretation of aircraft wind statistics assumes that the turbulence is isotropic and interprets the observed break at around 40 km as a transition between two isotropic regimes, in the reinterpretation, it is spurious and is simply a transition from horizontally to vertically dominated parts of the trajectory.

[43] In this paper, we have attempted to exploit this new understanding in order to both demonstrate and to quantify the wide-range horizontal scaling of the key atmospheric fields: wind, temperature, humidity, potential temperature. The basic theoretical framework for such wide-range scaling is anisotropic cascades; we demonstrate the horizontal cascade structure by directly analyzing the raw turbulent fluxes finding that they all follow a multiplicative cascade structure with external scales on the order of 10,000 km. Although this basic structure was present in all the analyzed fields, we noted the presence of the three different regimes predicted on the basis of their cross spectra with the aircraft altitude and with the pressure. The deviations were fairly strong for the wind and pressure which were strongly coupled with the trajectory, but relatively small for the temperature, humidity and potential temperature which were only weakly coupled. A rough summary is that at scales $< \approx 4$ km the trajectories vary smoothly but are affected by aircraft roll and pilot/autopilot controls, for scales ≈ 4–40 km the aircraft follow a rough, intermittent fractal trajectory; finally for scales ≥ 40 km the aircraft very closely follow the isobars which have significant vertical slopes. These regimes are for the ensemble statistics; the transition points vary considerably from trajectory to trajectory.

[44] Refined analyses of the statistics was performed by considering the scale by scale intermittency (characterized by the second-order moment of the flux) as well as the scale by scale smoothness of the fluctuations (characterized by the first-order structure function). It was argued that the optimum scale range for parameter estimation was ≈ 4–40 km where the intermittency in the altitude was not strong, the effect of the pilot/autopilot rolls was weak and the constraint of flying on an isobar was not yet so strong as to impose the verticals statistics on the wind field. We therefore used this range to give refined parameter estimates. Perhaps one of the most surprising results was the near identity of the scaling parameters H, C_1, α for temperature, log potential temperature and humidity, and in particular the nonstandard result $H = 0.51 \pm 0.01$ for all three fields which is extremely close to the fraction 1/2 but which nevertheless (apparently) still belies theoretical explanation (see, however, *Tuck* [2008]).

[45] Finally, we compared the estimates of the horizontal exponents with those from drop sondes of the corresponding vertical exponents. Overall, the ratios H_z for v, T, $\log\theta$, h were not far from the 23/9 D model prediction 5/9 (based on energy flux domination of horizontal statistics and buoyancy variance flux domination of vertical statistics), yet there were apparently systematic deviations: v, T, $\log\theta$ had $H_z \approx 0.47$ and for h, $H_z \approx 0.65$. For the moment, there is no satisfactory theoretical explanation for these results, although some clarification may come from a comparison with the structure of atmospheric reanalyses and (hydrostatic) numerical models which not only have nearly perfect cascade structures in the horizontal, but also at least some similar (and nonstandard) parameters including, at least for the ECMWF interim reanalysis, nearly identical spatial exponents for the isobaric wind exponents and the vertical sonde exponents. The fact that we find qualitatively (and in many cases quantitatively)

similar wide-range cascade structures in the simulations and in the atmosphere opens up new avenues for statistically verifying the models: their scale by scale statistics should be the quantitatively the same as those of the measurements.

[46] It is remarkable that in spite of the current golden age of meteorological observations there is still no scientific consensus about the atmosphere's basic scale by scale statistical properties, in particular those of the dynamical (wind) field. However, if we reinterpret the (systematically observed) transition from $\beta \approx 5/3$ to ≈ 2.4 spectral scaling in terms of a single anisotropic scaling turbulence, then there are no longer serious obstacles to the emergence of a consensus. To complete this emerging "new synthesis" [*Lovejoy and Schertzer*, 2010] the analyses presented here must be extended to the time domain, to different altitudes, and should be rechecked with different sensors and in particular to aircraft flying on isoheights. Perhaps most importantly, completion of the synthesis requires that we abandon the dogma of isotropy (or quasi-isotropy) and embark upon the systematic development of anisotropic but scaling theories of turbulence.

[47] **Acknowledgments.** We thank the crew of the Gulfstream 4 who gathered the data.

References

Bacmeister, J. T., et al. (1996), Stratospheric horizontal wavenumber spectra of winds, potential temperature, and atmospheric tracers observed by high-altitude aircraft, *J. Geophys. Res.*, *101*, 9441–9470, doi:10.1029/95JD03835.

Bartello, P. (1995), Geostrophic adjustment and inverse cascades in rotating stratified turbulence, *J. Atmos. Sci.*, *52*, 4410–4428, doi:10.1175/1520-0469(1995)052<4410:GAAICI>2.0.CO;2.

Boer, G. J., and T. G. Shepherd (1983), Large-scale two-dimensional turbulence in the atmosphere, *J. Atmos. Sci.*, *40*, 164–184, doi:10.1175/1520-0469(1983)040<0164:LSTDTI>2.0.CO;2.

Bolgiano, R., Jr. (1959), Turbulent spectra in a stably stratified atmosphere, *J. Geophys. Res.*, *64*, 2226–2229, doi:10.1029/JZ064i012p02226.

Charney, J. G. (1971), Geostrophic turbulence, *J. Atmos. Sci.*, *28*, 1087, doi:10.1175/1520-0469(1971)028<1087:GT>2.0.CO;2.

Chen, T.-C., and A. Wiin-Nielsen (1978), On non-linear cascades of atmospheric energy and enstrophy in a two-dimensional spectral index, *Tellus*, *30*, 313–322, doi:10.1111/j.2153-3490.1978.tb00846.x.

Chigirinskaya, Y., et al. (1994), Unified multifractal atmospheric dynamics tested in the tropics Part 1: Horizontal scaling and self organized criticality, *Nonlinear Processes Geophys.*, *1*, 105–114.

Cho, J., and E. Lindborg (2001), Horizontal velocity structure functions in the upper troposphere and lower stratosphere. 1. Observations, *J. Geophys. Res.*, *106*, 10,223–10,232, doi:10.1029/2000JD900814.

Dewan, E. (1997), Saturated-cascade similitude theory of gravity wave spectra, *J. Geophys. Res.*, *102*, 29,799–29,817, doi:10.1029/97JD02151.

Gagnon, J. S., et al. (2006), Multifractal earth topography, *Nonlinear Processes Geophys.*, *13*, 541–570.

Gao, X., and J. W. Meriwether (1998), Mesoscale spectral analysis of in situ horizontal and vertical wind measurements at 6 km, *J. Geophys. Res.*, *103*, 6397–6404, doi:10.1029/97JD03074.

Gardner, C. (1994), Diffusive filtering theory of gravity wave spectra in the atmosphere, *J. Geophys. Res.*, *99*, 20,601–20,622, doi:10.1029/94JD00819.

Gardner, C. S., et al. (1993), Gravity wave models for the horizontal wave number spectra of atmospheric velocity and density fluctuations, *J. Geophys. Res.*, *98*, 1035–1049, doi:10.1029/92JD02051.

Hamilton, K., Y. O. Takahashi, and W. Ohfuchi (2008), Mesoscale spectrum of atmospheric motions investigated in a very fine resolution global general circulation model, *J. Geophys. Res.*, *113*, D18110, doi:10.1029/2008JD009785.

Högström, U., et al. (1999), A case study of two-dimensional stratified turbulence, *J. Atmos. Sci. 56*, 959–976, doi:10.1175/1520-0469(1999)056<0959:ACSOTD>2.0.CO;2.

Koch, S. E., et al. (2005), Turbulence and gravity waves within an upper-level front, *J. Atmos. Sci.*, *62*, 3885–3908, doi:10.1175/JAS3574.1.

Kraichnan, R. H. (1967), Inertial ranges in two-dimensional turbulence, *Phys. Fluids*, *10*, 1417–1423, doi:10.1063/1.1762301.

Landahl, M. T., and E. Mollo-Christensen (1986), *Turbulence and Random Processes in Fluid Mechanics*, 154 pp., Cambridge Univ. Press, Cambridge, U. K.

Lilley, M., et al. (2004), 23/9 dimensional anisotropic scaling of passive admixtures using lidar aerosol data, *Phys. Rev. E*, *70*, 036307, doi:10.1103/PhysRevE.70.036307.

Lilley, M., et al. (2008), Scaling turbulent atmospheric stratification, Part II: Empirical study of the stratification of the intermittency, *Q. J. R. Meteorol. Soc.*, *134*, 301–315, doi:10.1002/qj.1202.

Lilly, D. K. (1989), Two-dimensional turbulence generated by energy sources at two scales, *J. Atmos. Sci.*, *46*, 2026–2030, doi:10.1175/1520-0469(1989)046<2026:TDTGBE>2.0.CO;2.

Lovejoy, S., and D. Schertzer (2010), Towards a new synthesis for atmospheric dynamics: Space-time cascades, *Atmos. Res.*, *96*, 1–52, doi:10.1016/j.atmosres.2010.01.004.

Lovejoy, S., D. Schertzer, and J. D. Stanway (2001), Direct evidence of planetary scale atmospheric cascade dynamics, *Phys. Rev. Lett.*, *86*(22), 5200–5203, doi:10.1103/PhysRevLett.86.5200.

Lovejoy, S., et al. (2004), Fractal aircraft trajectories and nonclassical turbulent exponents, *Phys. Rev. E*, *70*, 036306, doi:10.1103/PhysRevE.70.036306.

Lovejoy, S., A. F. Tuck, S. J. Hovde, and D. Schertzer (2007), Is isotropic turbulence relevant in the atmosphere?, *Geophys. Res. Lett.*, *34*, L15802, doi:10.1029/2007GL029359.

Lovejoy, S., et al. (2008a), The remarkable wide range scaling of TRMM precipitation, *Atmos. Res.*, *90*, 10–32, doi:10.1016/j.atmosres.2008.02.016.

Lovejoy, S., et al. (2008b), Scaling turbulent atmospheric stratification. I: Turbulence and waves, *Q. J. R. Meteorol. Soc.*, *134*, 277–300, doi:10.1002/qj.1201.

Lovejoy, S., D. Schertzer, V. Allaire, T. Bourgeois, S. King, J. Pinel, and J. Stolle (2009a), Atmospheric complexity or scale by scale simplicity?, *Geophys. Res. Lett.*, *36*, L01801, doi:10.1029/2008GL035863.

Lovejoy, S., A. F. Tuck, S. J. Hovde, and D. Schertzer (2009b), Vertical cascade structure of the atmosphere and multifractal dropsonde outages, *J. Geophys. Res.*, *114*, D07111, doi:10.1029/2008JD010651.

Lovejoy, S., et al. (2009c), Reinterpreting aircraft measurements in anisotropic scaling turbulence, *Atmos. Chem. Phys. Discuss.*, *9*, 3871–3920.

Mandelbrot, B. B. (1974), Intermittent turbulence in self-similar cascades: Divergence of high moments and dimension of the carrier, *J. Fluid Mech.*, *62*, 331–350, doi:10.1017/S0022112074000711.

Monin, A. S., and A. M. Yaglom (1975), *Statistical Fluid Mechanics*, MIT Press, Cambridge, Mass.

Nastrom, G. D., and K. S. Gage (1985), A climatology of atmospheric wavenumber spectra of wind and temperature by commercial aircraft, *J. Atmos. Sci.*, *42*, 950–960, doi:10.1175/1520-0469(1985)042<0950:ACOAWS>2.0.CO;2.

Ngan, K., et al. (2004), Three-dimensionalization of freely decaying two-dimensional flows, *Phys. Fluids*, *16*, 2918–2932, doi:10.1063/1.1763191.

Novikov, E. A., and R. Stewart (1964), Intermittency of turbulence and spectrum of fluctuations in energy-dissipation, *Izv. Akad. Nauk. Ser. Fiz.*, *3*, 408–412.

Obukhov, A. (1959), Effect of Archimedean forces on the structure of the temperature field in a turbulent flow, *Dokl. Akad. Nauk SSSR*, *125*, 1246–1248.

Palmer, T. (2001), A nonlinear dynamical perspective on model error: A proposal for non-local stochastic-dynamic parameterisation in weather and climate prediction models, *Q. J. R. Meteorol. Soc.*, *127*, 279–304.

Schertzer, D., and S. Lovejoy (1985), The dimension and intermittency of atmospheric dynamics, in *Turbulent Shear Flow 4*, edited by B. Launder, pp. 7–33, Springer, New York.

Schertzer, D., and S. Lovejoy (1987), Physical modeling and analysis of rain and clouds by anisotropic scaling of multiplicative processes, *J. Geophys. Res.*, *92*, 9693–9714, doi:10.1029/JD092iD08p09693.

Schertzer, D., and S. Lovejoy (1997), Universal multifractals do exist!: Comments on "A statistical analysis of mesoscale rainfall as a random cascade," *J. Appl. Meteorol.*, *36*, 1296–1303, doi:10.1175/1520-0450(1997)036<1296:UMDECO>2.0.CO;2.

Schertzer, D., et al. (1993), Generic multifractal phase transitions and self-organized criticality, in *Cellular Automata: Prospects in Astrophysical Applications*, edited by J. M. Perdang and A. Lejeune, pp. 216–227, World Sci., River Edge, N. J.

Skamarock, W. C. (2004), Evaluating mesoscale NWP models using kinetic energy spectra, *Mon. Weather Rev.*, *132*, 3019–3032, doi:10.1175/MWR2830.1.

Smith, K. S. (2004), Comment on: "The k^{-3} and $k^{-5/3}$ energy spectrum of atmospheric turbulence: Quasigeostrophic two-level model simulation," *J. Atmos. Sci.*, *61*, 937–941.

Stolle, J. (2009), Space-time Cascade structure of numerical models of the atmosphere, M.Sc. thesis, McGill Univ., Montreal, Que., Canada.

Stolle, J., et al. (2009), The stochastic cascade structure of deterministic numerical models of the atmosphere, *Nonlinear Process. Geophys.*, *16*, 1–15.

Strauss, D. M., and P. Ditlevsen (1999), Two-dimensional turbulence properties of the ECMWF reanalyses, *Tellus, Ser. A*, *51*, 749–772.

Szépfalusy, P., et al. (1987), Phase transitions associated with dynamical properties of chaotic systems, *Phys. Rev. A*, *36*, 3525, doi:10.1103/PhysRevA.36.3525.

Takahashi, Y. O., K. Hamilton, and W. Ohfuchi (2006), Explicit global simulation of the mesoscale spectrum of atmospheric motions, *Geophys. Res. Lett.*, *33*, L12812, doi:10.1029/2006GL026429.

Trenberth, K. E., and A. Solomon (1993), Implications of global atmospheric spatial spectra for processing and displaying data, *J. Clim.*, *6*, 531–545, doi:10.1175/1520-0442(1993)006<0531:IOGASS>2.0.CO;2.

Tuck, A. F. (2008), *Atmospheric Turbulence: A Molecular Dynamics Perspective*, Oxford Univ. Press, New York.

Tuck, A. F., et al. (2004), Scale Invariance in jet streams: ER-2 data around the lower-stratospheric polar night vortex, *Q. J. R. Meteorol. Soc.*, *130*, 2423–2444, doi:10.1256/qj.03.191.

VanZandt, T. E. (1982), A universal spectrum of buoyancy waves in the atmosphere, *Geophys. Res. Lett.*, *9*, 575–578, doi:10.1029/GL009i005p00575.

Yaglom, A. M. (1966), The influence on the fluctuation in energy dissipation on the shape of turbulent characteristics in the inertial interval, *Sov. Phys. Dokl., Engl. Transl.*, *2*, 26–30.

S. Lovejoy, Department of Physics, McGill University, 3600 University St., Montreal, QE H3A 2T8, Canada. (lovejoy@physics.mcgill.ca)

D. Schertzer, Université Paris Est, F-77455 Marne-la-Vallée CEDEX 2, France.

A. F. Tuck, Department of Physics, Imperial College London, London SW7 2AZ, UK.